doi.org/10.36721/PJPS.2026.39.2.REG.14829.1

AI-driven ANN and RSM-CCD integrated optimization of cinnarizine-domperidone bilayer tablet: *In-vitro* evaluation and *in-silico* PBPK modeling using GastroPlus®

Aatka Ali[1,2]*, Iyad Naeem Muhammad[1], Wajiha Iffat[3], Shumaila Tasneem[3], Syed Ahsan Ali[3], Sarah Jameel Khan[4] and Sidra Siddique[5]

[1]Department of Pharmaceutics, Faculty of Pharmacy and Pharmaceutical Sciences, University of Karachi, Pakistan
[2]Department of Pharmaceutics, Faculty of Pharmacy, Iqra University, Karachi, Pakistan
[3]Dow College of Pharmacy, Faculty of Pharmaceutical Sciences, DUHS, Karachi, Pakistan
[4]Department of Pharmacology, Faculty of Pharmacy, Hamdard University, Karachi
[5]Department of Pharmaceutics, Faculty of Pharmacy, Hamdard University, Karachi

Abstract: **Background**: Response surface methodology coupled with the design of experiments identifies the optimal response surface function related to selected independent factors. Due to their rigid structures, they lack the learning capability from the developed response function. In contrast, a more advanced artificial intelligence-based tool, artificial neural network (ANN), offers an alternative to RSM-based regression methods. **Objectives**: This study was conducted to investigate the combined application of experimental design and a neural computing framework for modeling and optimization of a bilayer tablet with biphasic release of cinnarizine (CNZ) and domperidone (DOM), followed by *in-silico* physiologically-based pharmacokinetic (PBPK) modeling. **Methods**: The experimental data from the trial formulations supported by the central composite design (CCD) were trained using an artificial neural network. The predicted values of the input variables (HPMC K4M, sodium carbonate, croscarmellose and magnesium stearate) targeting the output responses (% drug release at 1h, 6h, 12h, and friability) were cross-validated using the numerical and graphical optimization technique of CCD. The *in-silico* PBPK modeling was used to measure relative bioavailability and simulate *in-vivo* plasma profiles under fasting state through GastroPlus® software. **Results**: The optimum quantities for developing a bilayer tablet —15% HMPC K4M, 3% sodium carbonate, 2% croscarmellose, and 1% magnesium stearate — were found to be very similar by both the CCD and ANN models, with desirability values close to 1. Moreover, ANOVA revealed no statistically significant difference between the optimized and predicted formulations. GastroPlus® assisted in the relative bioavailability evaluation of the optimized bilayer formulation, with an immediate-release domperidone and an extended-release cinnarizine layer, showing 89% and 81%, respectively. **Conclusion**: It is concluded that AI-powered modeling, especially the integration of ANN, accelerates innovation, leading to faster and smarter optimization of pharmaceutical formulations.

Keywords: Artificial neural network (ANN); Central composite design; Machine learning; Physiologically-based pharmacokinetic modeling

Submitted on 10-07-2025 – Revised on 07-09-2025 – Accepted on 15-09-2025

INTRODUCTION

The advent of artificial intelligence has brought a revolutionary impact, leveraging vast amounts of data that surpass human efficiency. Precisely, Artificial intelligence (AI) deals with such cognitive tasks that humans usually manage. Machine learning (ML) is a specific field of AI based on learning methods that enable machines to learn from external data sources, just as humans do. Based on newly acquired knowledge, machine learning programs enhance their ability to process (Wang *et al*., 2022b). An artificial neural network (ANN) is an AI tool that resembles the human brain's working (Makomere *et al*., 2023). The multilayer perceptron (MLP), radial basis function neural networks (RBFNNs), convolutional neural networks (CNNs), Kohonen networks, and recurrent neural networks (RNNs) are a few familiar ANN models. Among them, CNNs are widely used for supervised learning of images, while RNNs are preferred for voice recognition. Kohonen networks, also known as self-organizing maps (SOMs), are applied in various domains of information, including speech recognition, classification, and clustering (Wang *et al*., 2022b).

Among the ANN techniques, the MLP is considered more efficient for building and predicting models. It is based on a feed-forward model composed of one input layer, one or more hidden layers, and one output layer (Pham *et al*., 2019). MLP's performance is its main advantage. The complex problem can be predicted and analyzed using an MLP, owing to its hidden layers, which possess problem-solving capability. The classification of unknown patterns is possible with the aid of known patterns that share the same properties, because MLPs solve problems probabilistically, providing approximate solutions to complex problems (Ismail *et al*., 2023). In addition, "feed-

**Corresponding author:* e-mail: aatka.ali@iqra.edu.pk

forward" does not imply that signals cannot be processed in the backward direction; rather, it indicates that the network architecture is loop-free. The backpropagation algorithm is also a key concept. Forward transmission of the signal and backpropagation of the error gradient are the two steps involved in training the backpropagation algorithm. It means that the calculated results are propagated from the input layer towards the output direction along with the acquisition of error signals. All the neurons in each layer receive the error signals from the output towards the input direction, once the weights and thresholds are calculated. All layers in MLP use the backward-pass error signal and employ gradient descent to recalculate each neuron's weights (Wang et al., 2022b).

Response surface methodology (RSM) is a statistical tool that uses empirical models to evaluate the effects of input variables on predefined output variables. The central composite design (CCD) is among the most widely used designs for fitting second-order models (Malenga *et al*., 2022). In the current study, a physiologically-based pharmacokinetic (PBPK) modeling software program is also implemented to predict *in-vivo* drug performance. PBPK software platforms are equipped with different mechanistic absorption frameworks, such as GastroPlus® is associated with Yu and Amidon's suggested compartmental absorption and transit model (CAT) (Yu and Amidon, 1999) that has been modified by incorporating many parameters, like colon absorption and is designated as advanced compartmental absorption and transit (ACAT) model (Demeester *et al*., 2023). This model comprises nine compartments that resemble the human GI tract and can predict the rate and extent of absorption in a similar manner (Lin *et al*., 2022). Based on physiological and biochemical diversity relative to healthy adults, a specific patient population can be built, and this virtual population can undergo further clinical trial simulations. Instead of performing a clinical trial, this strategy is appropriate for determining drug disposition in geriatrics (Vyas and Taft, 2025). PBPK modeling can expand the evidence base for pediatric dose regimens by combining with existing clinical pharmacokinetic data, which are often limited in number (Freriksen *et al*., 2023).

The building and the accuracy of the PBPK models are greatly affected by the unavailability of parameters. The parameters required to build a PBPK model can be categorized into physiological, drug-related, and experimentally generated parameters. Body weight, tissue perfusion rate, organ blood flow, tissue volume, and cardiac output are some of the physiological factors. Moreover, PBPK models are susceptible to factors related to the drug, such as chemical-specific absorption, distribution, metabolism, and excretion. Both crucial factors for PBPK can be obtained through expensive, lengthy experimental procedures. In addition, PBPK modeling is limited by the lack of in *vivo* data (Huang *et al*., 2024).

The present study employs a Quality by Design (QbD) approach based on RSM and a more modern machine learning tool, i.e., an artificial neural network (ANN), to optimize the formulation of a bilayer tablet containing domperidone (DOM) and cinnarizine (CNZ). Cinnarizine is a piperazine calcium blocker used to treat cerebrovascular problems (Zhang *et al*., 2022). Domperidone is a peripherally selective dopamine D2 receptor antagonist (Afzal *et al*., 2021). Motion sickness can be treated with a combination of these drugs. Based on clinical studies, the combination therapy of these medications was found to be more effective than the individual administration of each drug (Alam and Shakeel, 2024). Although research studies are available using the hybrid ML-ANN and RSM-CCD frameworks to predict predefined targets, the data lack information on the implementation of these approaches in a fixed-dose combination. The novelty of this work lies in integrating both methods into a fixed-dose combination bilayer tablet containing two different drugs with a dual-release profile, thereby supporting the QbD approach.

MATERIALS AND METHODS

Cinnarizine and domperidone maleate were provided as a gift sample from Aspin Pharma Pvt. Ltd. (Karachi, Pakistan). Acetonitrile was procured from Tedia (Fairfield, USA), ortho-phosphoric acid from BDH Chemicals, Ltd. (Poole, England), trimethylamine and magnesium stearate from Daejung chemicals and metals (Siheung-si, Gyeonggi-do, Korea), and Potassium hydroxide was purchased from Merck (Darmstadt, Germany). Hydroxypropyl methyl cellulose (HPMC) K4M, potassium dihydrogen phosphate, sodium carbonate, and PVP-K30 were procured from Sigma-Aldrich (Steinheim, Germany). Avicel PH-101 and croscarmellose were obtained from Avonchem (Cheshire, United Kingdom), and Iron oxide yellow (E172) was procured from Evonik Industries (Givaudan Roure, GmbH, Germany).

Experimental design for the CNZ and DOM formulations

The RSM-based CCD was applied to statistically analyze two factors per layer at five levels, i.e., +1, -1, 0, +α, and -α (where α = 1.414), employing Design-Expert® (State-Ease, 360 trial version, Inc., Minneapolis, MN 55413, USA). The selected independent and dependent factors, their levels, and the output responses, along with their constraints, are compiled in table 1. The central composite design based on randomization included four axial, four factorial, and centre-point runs, each repeated quintuply, to evaluate the method's repeatability. The experimental runs were determined by 2^k+2k+n_0, where k and n_0 denote the numbers of independent variables and repetitions at the centre point, respectively (Mazumdar *et al*., 2021). A total of 13 trial batches of each extended-release cinnarizine (ER) and immediate-release domperidone (IR)

formulations corresponding to F1-F13 and FD1-FD13, respectively, were generated keeping k=2 and n=5 (Table 2).

Pre-compression and compatibility studies

The micrometrics studies were conducted to assess the flow characteristics of all the trial batches generated by CCD (Table 2) as per USP-NF specifications (USP-NF, 2022). A known quantity of the powder blend was weighed into a 10ml graduated cylinder to determine the bulk density, and the powder was mechanically tapped until a constant volume was reached to determine the tapped density. The following equations were used to calculate the parameters, including tapped density (ρ_t), bulk density (ρ_b), Carr's index, Hausner's ratio, and angle of repose.

$$\text{Bulk density } (\rho_b) = \frac{\text{Mass of powder(g)}}{\text{Volume of powder(ml)}} \quad (1)$$

$$\text{Tapped density } (\rho_t) = \frac{\text{Mass of powder(g)}}{\text{Tapped volume(ml)}} \quad (2)$$

$$\text{Carr's index} = \frac{(\rho_t - \rho_b)}{\rho_t} \times 100 \quad (3)$$

$$\text{Hausner's ratio} = \frac{\text{Tapped density } (\rho t)}{\text{Bulk density } (\rho_b)} \quad (4)$$

$$\text{Angle of repose } (\theta) = \tan^{-1}\frac{2h}{d} \quad (5)$$

Where "h" and "d" are the height and diameter of the heap, respectively.

The interaction between drugs with the polymer and superdisintegrant was determined by Fourier transform infrared (FTIR) spectrometry (Nicolet-6700, Thermo Scientific, US) in the region of 4000-400 cm^{-1}. The physical mixture of cinnarizine and HPMC K4M, as well as domperidone and croscarmellose, at a 1:1 ratio was analyzed (Rojek *et al*., 2023).

Preparation of the extended-release (ER) layer of CNZ

The extended-release (ER) layer was prepared by the wet granulation method using a single-punch machine (Erweka, Korsch, Frankfurt, Germany) fitted with an eccentric B-type biconvex punch and die set (11.5 mm diameter). All the ingredients (Table 2) were accurately weighed and passed through the stainless steel sieve (mesh no. 25) separately. The drug (CNZ), HPMC K4M, sodium carbonate, microcrystalline cellulose, and iron oxide yellow pigment were thoroughly mixed. The aqueous granulating fluid of PVP-K-30 (5% w/w) was added to the powder blend dropwise till a suitable wet mass was obtained, followed by granulation through sieve 12. The obtained granules were oven-dried at 60 ºC for 1h and then sieved through a 30 screen. The final dried granules were blended with magnesium stearate before compression.

Preparation of the immediate-release (IR) layer of DOM

The granules for the immediate-release layer were prepared using the same procedure as for the ER layer. The accurately weighed ingredients (Table 2) were blended and granulated with 10% (w/w) aqueous PVP-K-30, then oven dried and sieved. Magnesium stearate was blended with the granules prior to compression (Prajapati *et al*., 2009).

Preparation of a bilayer tablet of CNZ and DOM

The bilayer tablet formulation (B1) was prepared by the double-compression technique using the optimized layers of DOM and CNZ, with acceptable dissolution profiles. Initially, the extended-release layer of CNZ granules was fed into the die cavity and then compressed to achieve an intermediate tablet with an average weight of ± 200 mg using a B-type biconvex (11.5 mm diameter) single-punch machine (Erweka, Korsch, Frankfurt, Germany). The granules of the immediate-release (IR) layer were then poured over the pre-compressed intermediate extended-release layer, subsequently compressed to an average weight of ± 400 mg (Nguyen *et al*., 2021).

Post-compression quality control evaluation

Each trial and optimized formulations of both drugs (FD1-FD13), (F1-F13), and (B1) were subjected to quality control evaluation. The weight variation and friability of the tablets were determined by using an analytical balance (Sartorius CP224S, Germany) and a Roche-type friabilator (Erweka GmbH, Heusenstamm, Germany), respectively. The diameter and thickness were measured using a vernier caliper (Seiko, China). The hardness and disintegration time of tablets were measured by a hardness tester (Erweka, Germany) and a basket rack disintegration assembly (Erweka ZT2, Heusenstamm, Germany), respectively (USP-NF, 2022; Asrade *et al*., 2023).

In-vitro dissolution study and release kinetics

All the trial formulations were subjected to in vitro drug release studies using the USP paddle-type apparatus (Erweka GmbH 600, Heusenstamm, Germany). The tablets were placed in hemispherical dissolution vessels containing 900 mL of 0.1N HCl (pH 1.2) at 50 rpm. The dissolution medium was maintained at 37±0.5°C and the samples (10 ml) were drawn at regular time intervals (0.5, 1, 2, 3, 4, 5, 6, 7, 8, 9, 10, 11 and 12 h) for ER tablets (CNZ) while 1h (5, 10, 20, 30, 45 and 60 min) for IR tablets (DOM). The same volume withdrawn each time was replaced with fresh dissolution medium. All the samples were filtered through a 0.45µm Whatman filter paper and the resultant filtrates were diluted. The samples of cinnarizine and domperidone were analyzed by using a UV-spectrophotometer (UV-1800, Shimadzu Corporation, Kyoto, Japan) at 254nm (Kesharwani and Ibrahim, 2023) and 284nm (Ardalkar *et al.,* 2024) respectively.

Table 1: Selection of factors, levels, responses and constraints of the extended and immediate release formulations for CCD-based optimization

Variables	Levels	
Independent variables (Extended-release formulation, CNZ)	*Low*	*High*
X_1= HPMC K4M	*5*	*25*
X_2= Sodium carbonate	*3*	*5*
Dependent Variables (Extended-release formulation, CNZ)	Constraints	
Y_1= Cumulative % drug Release in 1h	13.9%<Y_1<20%	
Y_2= Cumulative % drug Release in 6h	50%<Y_2<70%	
Y_3= Cumulative % drug Release in 12h	90%<Y_3<100%	
Independent Variables (Immediate-release formulation, DOM)	Low	*High*
X_1= Croscarmellose	1	3
X_2= Magnesium stearate	0.5	1.5
Dependent variables (Immediate-release formulation, DOM)	Constraints	
Y_1= Cumulative % drug release in 1h	85%< Y_1<100%	
Y_2= Friability	0%< Y_2<1%	

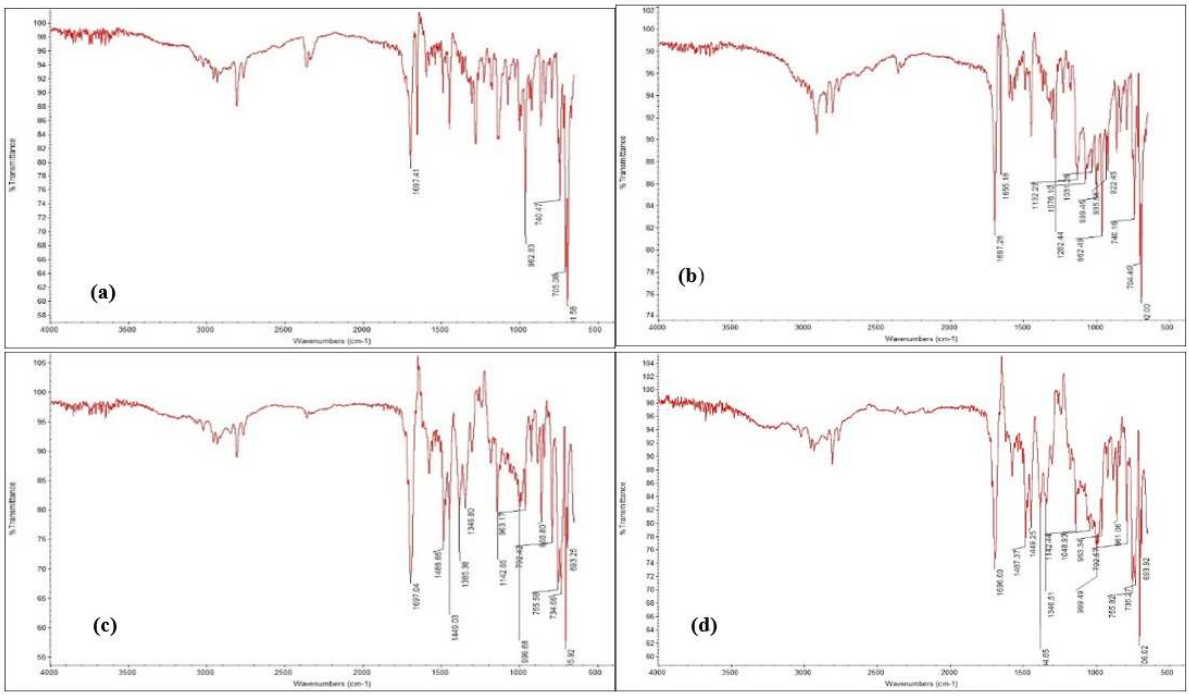

Fig. 1: FTIR spectra (a) Pure API (cinnarizine) (b) Cinnarizine and polymer (HPMC K4M) (c) Pure API (domperidone) (d) Domperidone and superdisintegrant (croscarmellose)

To examine the drug release mechanism from the ER tablet, an Excel add-in program, DD solver, was used to apply a model-dependent approach, including zero-order, first-order, Higuchi, Hixson Crowell, and Korsmeyer Peppas models, whereas first-order and Hixson Crowell models were applied to examine the release profiles of IR tablets (Maqbool *et al*., 2024).

$$Q_t = Q_o + K_o t \text{ (Zero Order)} \quad (6)$$

$$Q_t = Q_o^{e^{-k_1 t}} \text{ (First order)} \quad (7)$$

$$Q_t = k_H t^{0.5} \text{ (Higuchi)} \quad (8)$$

$$Q_o^{1/3} - Q_t^{1/3} = K_{HC} t \text{ (Hixon Crowell)} \quad (9)$$

$$M_t / M_\infty = K_{kp} t^n \text{ (Korsmeyer Peppas)} \quad (10)$$

Where, Q_t = the amount of drug released at time (t), Q_o = the initial amount of drug released at time (t=0), K_o = zero order rate constant, k_1= first order rate constant, k_H = Higuchi constant K_{HC} =Hixson Crowell constant, M_t/M_∞ is the fraction of drug release at time (t), k= kinetic constant and n= diffusion exponent

Model-independent methods

The similarity in dissolution profiles of IR and ER tablets of the trial formulations was assessed using the f_2 similarity factor in DD solver, with 0.1 N HCl buffer (pH 1.2) as the dissolution medium. Formulations were considered similar in terms of dissolution profile if the calculated f_2 value was ≥ 50 (Diaz *et al*., 2016).

Table 2 Composition of the extended-release ER (CNZ) and immediate-release IR (DOM) layers

Sample Code ER layer	CNZ mg	HPMC K4M mg (%)	Sodium carbonate mg (%)	Iron oxide pigment (mg)	Magnesium stearate (mg)	PVP K30 (mg)	Avicel® PH 101 (mg)	Sample Code IR layer	DOM[a] (mg)	Croscarmellose mg (%)	Magnesium stearate mg (%)	PVP K30 (mg)	Avicel® PH 101 (mg)
F1	75	30(15)	8(4)	2	2	10	73	FD1	19.1	1.18(0.59)	3(1.5)	20	157
F2	75	30(15)	10.82(5.41)	2	2	10	70	FD2	19.1	4(2)	3(1.5)	20	154
F3	75	30(15)	8(4)	2	2	10	73	FD3	19.1	4(2)	3(1.5)	20	154
F4	75	1.72(0.86)	8(4)	2	2	10	101	FD4	19.1	4(2)	3(1.5)	20	154
F5	75	30(15)	8(4)	2	2	10	73	FD5	19.1	2(1)	2(1)	20	157
F6	75	30(15)	8(4)	2	2	10	73	FD6	19.1	6(3)	2(1)	20	153
F7	75	30(15)	5.18(2.59)	2	2	10	75	FD7	19.1	4(2)	1.58(0.79)	20	155
F8	75	30(15)	8(4)	2	2	10	73	FD8	19.1	2(1)	4(2)	20	155
F9	75	58.28(29.14)	8(4)	2	2	10	44	FD9	19.1	6(3)	4(2)	20	151
F10	75	10(5)	10(5)	2	2	10	91	FD10	19.1	4(2)	4.42(2.21)	20	152
F11	75	10(5)	6(3)	2	2	10	95	FD11	19.1	6.82(3.41)	3(1.5)	20	151
F12	75	50(25)	6(3)	2	2	10	55	FD12	19.1	4(2)	3(1.5)	20	154
F13	75	50(25)	10(5)	2	2	10	51	FD13	19.1	4(2)	3(1.5)	20	154

[a]Domperidone maleate is added at 19.1 mg per layer, which is equivalent to 15 mg domperidone base

Assay of the developed optimized formulation

The assay of the optimized formulation (B1) was performed using a modified HPLC method as described by Clark (Conemans, 2011). The HPLC system consisted of an isocratic pump (LC-20AT, Shimadzu, Kyoto, Japan) fitted with a C-18 column (ODS-H optimal 5µm, 150 x 4.6 mm i.d.), UV-visible detector (SPD-20A, Shimadzu, Kyoto, Japan), auto-sampler (SIL-20 A $_{HT}$, Shimadzu, Kyoto, Japan), and a column oven (CTO-20A). Data acquisition and processing were performed using Lab Solutions software (version 5.65, Shimadzu Corporation). The column oven was kept at ambient temperature, and the pump was set to a flow rate of 1.3 ml/min with an injection volume of 40 µl. A mixture of acetonitrile and buffer (pH 3.3) at a 47:53 ratio was used as the mobile phase. The buffer was prepared by adding orthophosphoric acid (750 µl) and triethylamine (approx. 150 µl) to distilled water, and the potassium hydroxide solution (10%) was used to adjust the pH. The mobile phase was then filtered through a 0.45µm membrane filter using a filtration assembly, and degassed in an ultrasonicator (Ultrasonic LC-10 H, Elma, Germany) for 15-20 minutes. The peaks of eluents were detected at 210 nm.

Comparison between CCD and ANN-based modeling

In the present work, a multilayer perceptron artificial neural network (MLP-ANN) was applied to the experimental data sets of each ER and IR tablet using JMP® Pro 18 software (SAS Institute Inc., North Carolina, USA) (Navabhatra *et al*., 2021; Paneiro and Rafael, 2021). The ANN model findings were also cross-validated against graphical and numerical optimization of the RSM-based CCD using Design-Expert® (Saleem *et al*., 2025). The optimized formulations were subsequently used to prepare a bilayer tablet.

ANN topology

The MLP-ANN architecture was built using supervised training and testing on the experimental data sets generated by CCD for both ER and IR formulations. The ANN models were crafted in three layers. The input layer of the ER formulation consists of two neurons, representing the independent variables, i.e., HPMC K4M (X_1) and sodium carbonate (X_2). In comparison, the output layer consists of three neurons, considered as dependent variables: % drug release at 1h (Y_1), 6h (Y_2), and 12h (Y_3). Both layers are interconnected, with a single hidden layer, and all nodes use the hyperbolic tangent (TanH) as their activation function. Similarly, the input layer of IR formulations comprises two neurons — croscarmellose (X_1) and magnesium stearate (X_2) —while the output layer comprises two neurons, presenting % drug release at 60 min (Y_1) and friability (Y_2). The feed-forward back propagation algorithm was applied to train and test the multilayer perceptron.

Table 3 Micromeritic studies of the trial batches of IR (FD1-FD13) and ER (F1-F13) tablets

Sample Code	Bulk volume (ml)	Tapped volume (ml)	Bulk density (g/ml)	Tapped density (g/ml)	Hausner's ratio (HR)	Compressibility index (CI) (%)	Angle of repose (θ)	Interpretation (USP-NF., 2022)
IR tablets (DOM)								
FD1	4.00	3.91	0.37	0.38	1.02	2.50	28	Excellent (HR and CI), Good (θ)
FD2	3.50	3.20	0.42	0.46	1.09	8.57	29	Excellent (HR and CI), Good (θ)
FD3	4.40	4.20	0.34	0.35	1.04	4.54	31	Excellent (HR and CI), Fair (θ)
FD4	3.60	3.20	0.41	0.46	1.12	11.11	25	Good (HR), Good (CI and θ)
FD5	4.20	4.11	0.35	0.36	1.02	2.38	26	Excellent (HR and CI), Good (θ)
FD6	4.41	4.00	0.34	0.37	1.11	9.09	26	Excellent (HR and CI), Good (θ)
FD7	3.51	3.21	0.42	0.46	1.09	8.57	25	Excellent (HR and CI), Good (θ)
FD8	4.41	4.24	0.34	0.35	1.04	4.54	26	Excellent (HR and CI), Good (θ)
FD9	3.62	3.21	0.41	0.46	1.12	11.11	26	Good (HR), Good (CI and θ)
FD10	4.23	4.11	0.35	0.36	1.02	2.38	25	Excellent (HR and CI), Good (θ)
FD11	4.42	4.01	0.34	0.37	1.11	9.09	25	Excellent (HR and CI), Good (θ)
FD12	4.10	4.01	0.36	0.37	1.02	2.43	31	Excellent (HR and CI), Fair (θ)
FD13	4.50	4.21	0.33	0.35	1.07	6.66	29	Excellent (HR and CI), Good (θ)
ER tablets (CNZ)								
F1	3.80	3.40	0.39	0.44	1.11	10.5	33	Excellent (HR and CI), Fair (θ)
F2	3.11	3.10	0.89	0.92	1.03	3.22	32	Excellent overall
F3	3.81	3.10	0.74	0.91	1.22	18.4	22	Fair (HR and CI), Excellent (θ)
F4	3.31	3.10	0.30	0.33	1.11	9.09	36	Excellent (HR and CI), Passable (θ)
F5	3.41	3.21	0.29	0.31	1.06	5.88	36	Excellent (HR and CI), Passable (θ)
F6	4.40	4.10	0.28	0.31	1.11	9.09	27	Excellent (HR and CI), Good (θ)
F7	3.90	3.71	0.39	0.41	1.05	5.12	26	Excellent overall
F8	3.80	3.41	0.39	0.44	1.11	10.52	33	Excellent (HR and CI), Fair (θ)
F9	3.10	3.03	0.89	0.92	1.03	3.22	32	Excellent overall
F10	3.80	3.11	0.74	0.91	1.22	18.42	22	Fair (HR and CI), Excellent (θ)
F11	3.30	3.10	0.30	0.33	1.11	9.09	36	Excellent (HR and CI), Passable (θ)
F12	3.40	3.20	0.29	0.31	1.06	5.88	36	Excellent (HR and CI), Passable (θ)
F13	4.40	4.01	0.28	0.31	1.11	9.09	27	Excellent (HR and CI), Good (θ)

Table 4 Quality control attributes of IR (FD1-FD13), ER (F1-F13) and a bilayer formulation (B1 with two optimized layers Fopt. CCD (DOM), Fopt. CCD (CNZ))

Quality control attributes	FD1	FD2	FD3	FD4	FD5	FD6	FD7	FD8	FD9	FD10	FD11	FD12	FD13
Weight variation* (mg) (n=20)	203 ±1.72	201 ±1.93	204 ±1.97	202 ±1.87	205 ±1.33	200 ±2.16	201 ±2.09	200 ±1.23	200 ±0.88	201 ±1.63	202 ±1.98	202 ±1.73	201 ±2.48
Diameter* (mm) (n=20)	11.31 ±0.13	11.32 ±0.15	11.09 ±2.42	11.38 ±0.02	11.29 ±0.11	11.11 ±0.16	11.08 ±0.02	11.06 ±0.02	11.11 ±0	11.11 ±0.06	11.11 ±0.06	11.12 ±0.04	11.10 ±0.02
Thickness* (mm) (n=20)	3.20 ±0.11	3.21 ±0.14	3.31 ±0.01	3.31 ±0.01	3.28 ±0.1	3.11 ±0.16	3.05 ±0	3.06 ±0.02	3.08 ±0.04	3.11 ±0.06	3.06 ±0.02	3.11 ±0	3.05 ±0
Hardness* (kg/cm²) (n=20)	3.12 ±0.20	3.10 ±0.11	3.47 ±0.05	3.81 ±0	3.91 ±0.10	4.00 ±0.20	4.11 ±0	4.21 ±0.10	3.51 ±0.20	4.61 ±0.20	4.51 ±0.50	4.51 ±0.50	4.20 ±0.50
Disintegration* (sec) (n=6)	20 ±0.03	10 ±0.04	10 ±0.05	10 ±0.06	8 ±0.02	4 ±0.09	6 ±0.07	12 ±0.08	4 ±0.09	10 ±0.09	4 ±0.09	10 ±0.09	10 ±0.08
Friability (%) (n=20)	0.30	0.40	0.15	0.16	0.10	0.50	0.50	0.40	0.50	0.60	0.80	0.90	0.80
	F1	F2	F3	F4	F5	F6	F7	F8	F9	F10	F11	F12	F13
Weight variation* (mg) (n=20)	202 ±4	205 ±3.7	203 ±4.3	203 ±4.3	204 ±4.8	204 ±4.4	204 ±4.4	204 ±3.8	205 ±3.3	203 ±2.43	204 ±2.4	206 ±1.27	204 ±2.15
Diameter* (mm) (n=20)	11.13 ±0.08	11.25 ±0.22	11.45 ±0.09	11.4 ±0.06	11.3 ±0.06	11.17 ±0.06	11.37 ±0.21	11.37 ±0.21	11.08 ±0.02	11.18 ±0.02	11.17 ±0.06	11.17 ±0.06	11.18 ±0.02
Thickness* (mm) (n=20)	3.31 ±0.13	3.21 ±0.15	3.21 ±0.15	3.15 ±0.05	3.15 ±0.05	3.12 ±0.04	3.16 ±0.07	3.16 ±0.07	3.12 ±0.02	3.12 ±0.05	3.09 ±0.01	3.09 ±0.01	3.07 ±0.03
Hardness* (kg/cm²) (n=20)	6.10 ±0.1	5.77 ±0.12	6.00 ±0	5.80 ±0.2	5.8 ±0.2	6.80 ±0.1	5.70 ±0.2	5.60 ±0.2	6.00 ±0	5.50 ±0	6.50 ±0.2	5.50 ±0.3	6.01 ±0.1
Friability (%) (n=20)	0.24	0.19	0.15	0.16	0.11	0.11	0.30	0.40	0.50	0.60	0.70	0.90	0.50
	B1 (bilayer tablet)												
	Fopt. CCD (DOM)					Fopt. CCD (CNZ)							
Weight variation* (mg) (n=20)	402.55±0.97												
Diameter* (mm) (n=20)	11.16±0.09												
Thickness* (mm) (n=20)	5.34±0.13												
Hardness* (kg/cm²) (n=20)	7.70±0.12												
Friability (%) (n=20)	0.60												
Assay* (n=6)	99.00±0.50					100.01±0.300							

*Expressed as Mean ± SD

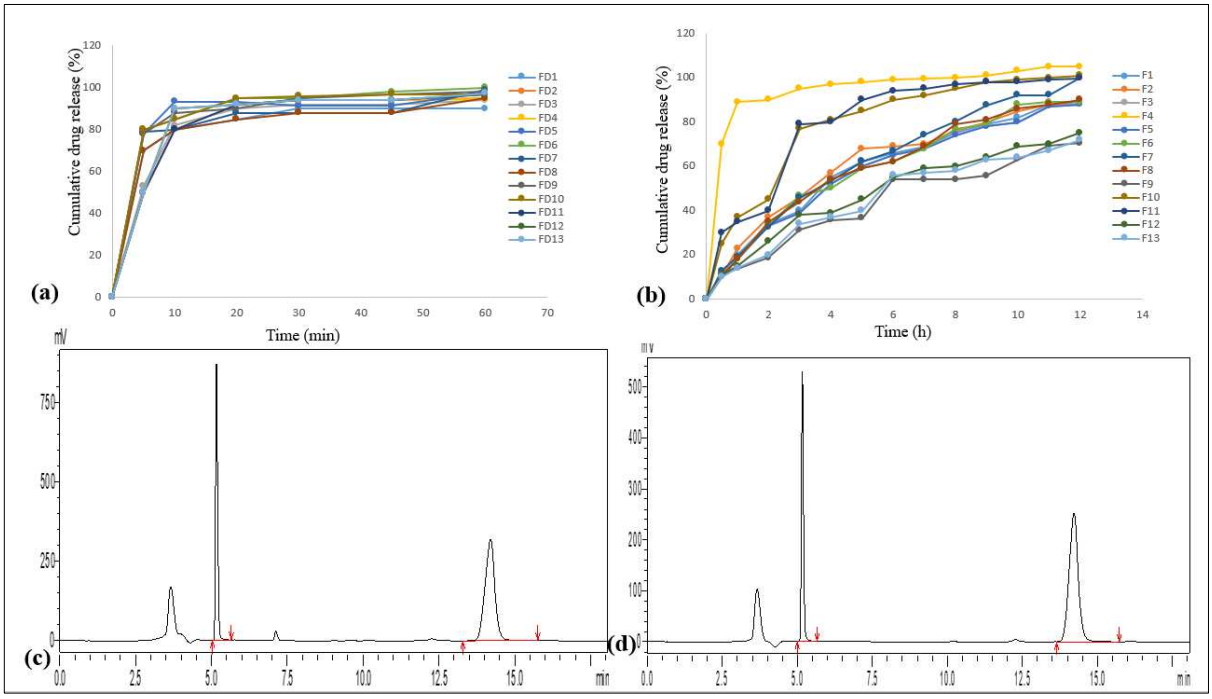

Fig. 2: Cumulative % drug release vs. time profiles (a) IR formulations (DOM) (b) ER formulations (CNZ) (c) Standard chromatogram of DOM and CNZ (d) Chromatogram of a optimized bilayer tablet (B1)

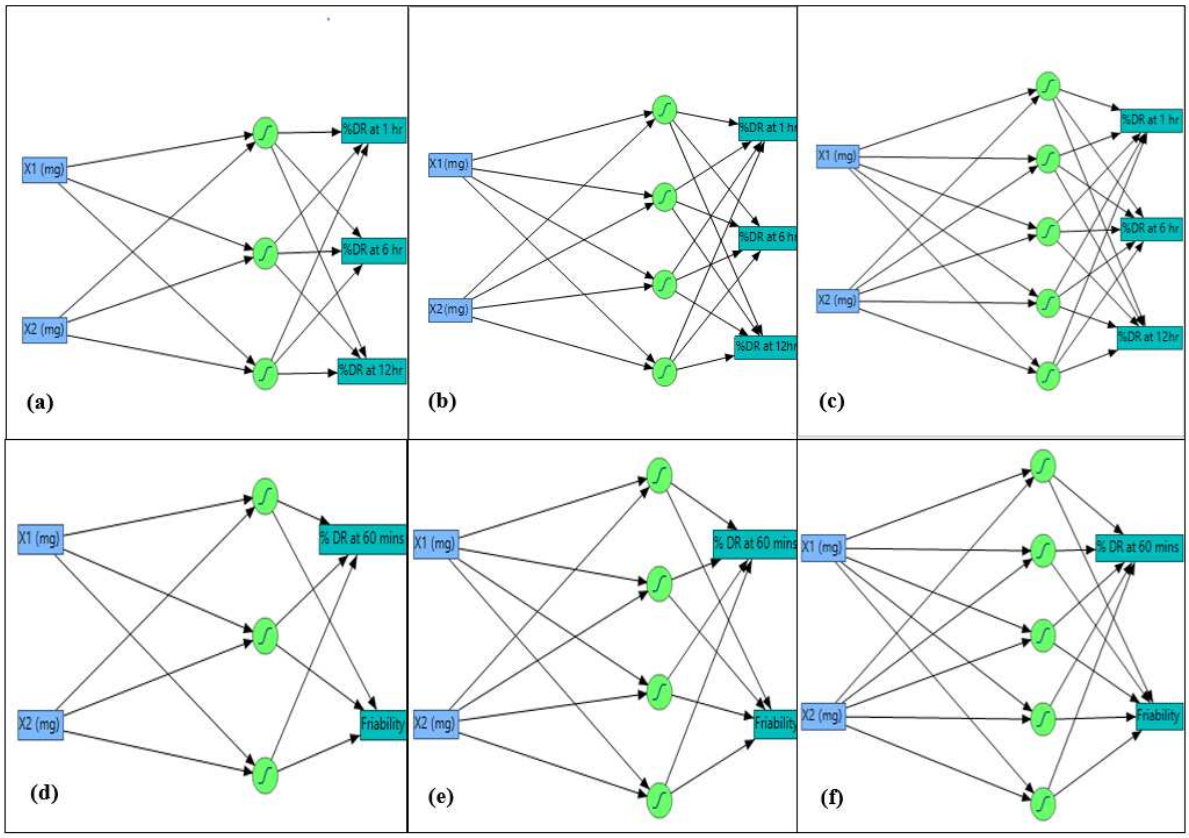

Fig. 3: MLP neural network topologies (a–c) ER formulations of CNZ with inputs (X_1 =HPMC K4M, X_2=sodium carbonate) and outputs %DR at 1h, 6h, and 12h, (d–f) IR formulations of DOM with inputs (X_1=croscarmellose, X_2=magnesium stearate) and outputs % DR at 60 mins and friability using 3, 4 and 5 hidden nodes respectively

Table 5 Drug release kinetics of the ER (F1-F13) and IR (FD1-FD13) formulations using model-independent and dependent approaches

Sample code ER	Zero Order	First order		Higuchi		Korsmeyer- Peppas			Hixon Crowell		[a]f_2	Sample code IR	First order		Hixon Crowell		[b]f_2
	r^2	k_0	r^2	k_1	r^2	k_H	r^2	k_{KP}	n	r^2	k_{HC}				r^2	k_{HC}	
F1	0.74	8.90	0.99	0.18	0.98	26.0	0.98	23.4	0.55	0.96	0.04	62.95*	FD1	0.91	0.19	0.60	0.02	50.83*
F2	0.63	9.09	0.98	0.19	0.97	26.79	0.97	26.45	0.50	0.94	0.05	63.36*	FD2	0.98	0.14	0.84	0.02	64.31*
F3	0.78	8.74	0.99	0.17	0.97	25.55	0.98	22.06	0.57	0.97	0.04	59.8*	FD3	0.97	0.15	0.80	0.02	60.84*
F4	0.30	1.16	0.48	2.29	0.60	37.86	0.97	83.04	0.09	0.76	0.13	21.34	FD4	0.97	0.16	0.78	0.02	57.95*
F5	0.78	8.74	0.99	0.17	0.97	25.55	0.98	22.06	0.57	0.97	0.04	59.8*	FD5	0.97	0.29	0.50	0.02	47.25
F6	0.79	8.96	0.98	0.18	0.97	26.16	0.98	22.36	0.57	0.97	0.04	65.45*	FD6	0.98	0.28	0.58	0.02	50.66*
F7	0.83	9.59	0.98	0.20	0.97	27.93	0.99	22.67	0.60	0.98	0.05	-	FD7	0.90	0.24	0.54	0.02	47.68
F8	0.78	9.01	0.99	0.18	0.97	26.34	0.98	22.88	0.57	0.97	0.05	67.12*	FD8	0.91	0.19	0.62	0.02	51.14*
F9	0.85	6.69	0.96	0.10	0.94	19.42	0.97	14.83	0.63	0.94	0.03	34.36	FD9	0.97	0.27	0.57	0.02	50.77*
F10	0.01	11.14	0.97	0.40	0.85	33.43	0.91	43.24	0.37	0.95	0.10	38.14	FD10	0.97	0.27	0.56	0.02	50.28*
F11	0.07	11.21	0.94	0.41	0.80	33.69	0.87	44.24	0.36	0.93	0.10	36.55	FD11	0.98	0.14	0.85	0.02	65.88*
F12	0.78	7.26	0.97	0.12	0.97	21.23	0.98	18.32	0.57	0.93	0.03	39.65	FD12	0.97	0.16	0.79	0.02	59.21*
F13	0.82	6.94	0.97	0.11	0.95	20.21	0.97	16.21	0.60	0.94	0.03	36.55	FD13	0.97	0.16	0.79	0.02	59.43*

[a]F7 formulation was considered as the reference formulation for the determination of the f_2 factor, owing to its quality control attributes in case of ER tablets, [b]A1 (marketed product) was used as the reference formulation for IR tablets. Values indicating asterisk (*) show similarity as per FDA recommendation i.e., 50-100 (Altoum et al., 2024).

The holdback procedure was used at a 0.3 (70:30) split by selecting from the model launch menu, as it randomly divides the dataset into training (70%) and testing (30%) (Simões et al., 2020; Wang *et al*., 2022a). The hidden neurons and learning rate were examined using the squared penalty method to determine the optimized ANN architecture (Elsayed *et al*., 2021; El-Metwally *et al*., 2023). The neural nodes were tested in the range of 3-5 (Paneiro and Rafael, 2021). The sum of squared errors (SSE) and the r^2 values were used to assess the predictive ability and statistical significance of the ANN model (Simões *et al*., 2020).

Implementation of the desirability function for ANN-based optimization

To obtain optimized formulations, the best node was selected based on the maximum r^2 and minimum SSE. For the selected node, a prediction profiler was computed using the built-in model profiler in JMP® Pro 18, and the desirability function for each response was applied based on response limits (Harkat-Madouri *et al*., 2025). The predicted formulations of both drugs, $F_{pred.\ ANN}$ (CNZ) and $F_{pred.\ ANN}$ (DOM) models were formulated in JMP® Pro 18, and the critical output responses were analyzed along with other quality control attributes (Khan *et al*., 2023).

Implementation of the desirability function for CCD-based optimization

The same experimental data sets were estimated by numerical and graphical optimization of CCD based on the desirability approach. The polynomial equations coupled with quadratic terms were established by multiple linear regression analysis (MLRA). At the 5% significance level, the model terms' significance was determined (Akhtar *et al*., 2024). The ramp and overlay plots were constructed to present the design space and to predict the desired quantities for optimal responses.

Analysis of variance for the comparison of optimized and predicted formulations

To cross-validate, the optimized formulations, i.e., $F_{opt.\ CCD}$ (CNZ) and $F_{opt.\ CCD}$ (DOM), suggested by employing numerical and graphical optimization techniques, was compared with $F_{pred.\ ANN}$ (CNZ) and $F_{pred.\ ANN}$ (DOM) formulations assisted by a trained ANN model. The proposed formulations were prepared in triplicate and assessed for the output responses, which were subsequently compared using one-way analysis of variance in SPSS version 25 at the 5% significance level.

In-silico PBPK modeling

Model building

A PBPK model was developed using the built-in 'Advanced Compartmental Absorption and Transit' (ACAT)® model in GastroPlus® software version 9.9 (Simulations Plus Inc., Lancaster, CA, USA) to estimate $F_{opt.\ CCD}$ (CNZ) and $F_{opt.\ CCD}$ (DOM).

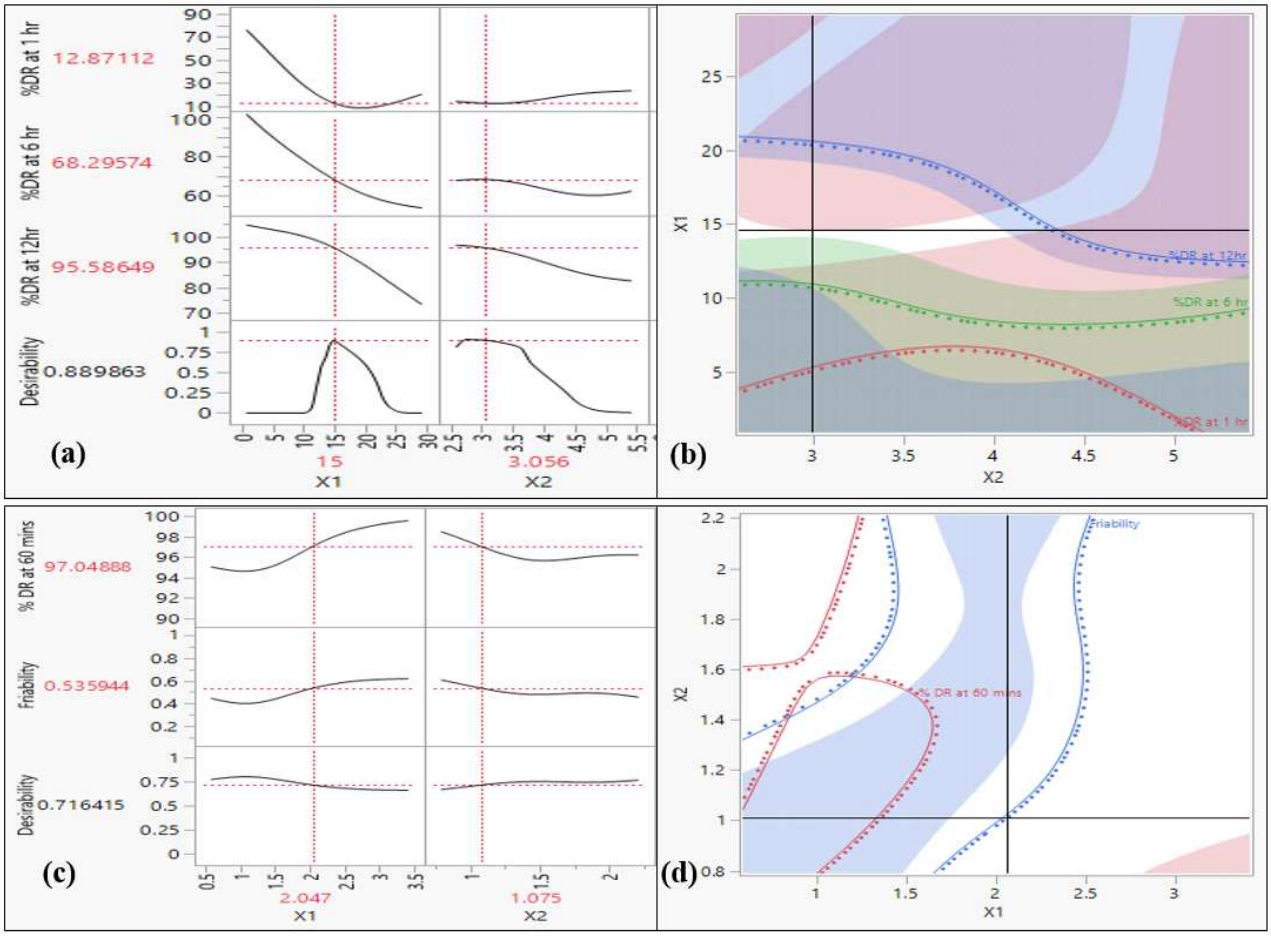

Fig. 4: Profiler based on desirability function computed by ANN topology (a) Prediction profiler of the ER formulations (b) Contour profiler for the ER formulations (c) Prediction profiler of the IR formulations (d) Contour profiler for the IR formulations

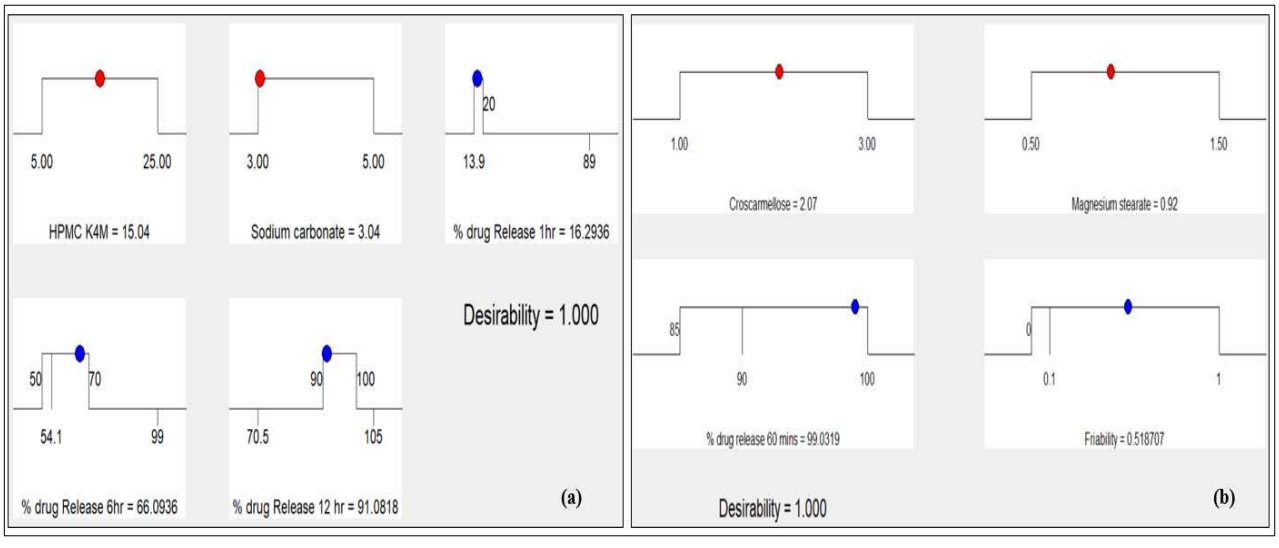

Fig. 5: Selected CCD-generated ramp plots with desirability values for the optimized (a) Extended-release (ER) formulation (CNZ) (b) Immediate-release (IR) formulation (DOM)

Table 6: Performance indices of the MLP-ANN architecture

Nodes	Data set ER tablets (CNZ)	Generalized r^2	% drug release 1 h (Y_1)		% drug release 6 h (Y_2)			
			r^2	SSE	r^2	SSE	r^2	SSE
3	Training	0.98	0.84	730.7	0.97	63.4	0.99	12.4
	Testing	0.96	0.84	4.59	0.7	32.16	0.05	126.1
4*	Training	1.00	0.87	58.4	0.98	36.77	0.97	35.2
	Testing	0.90	0.86	14.7	0.83	52.04	0.83	62.4
5	Training	0.99	0.74	117.6	0.97	65.3	0.95	50.65
	Testing	0.80	-2.06	104.1	0.80	21.7	0.67	43.1
Nodes	Data set IR tablets (DOM)	Generalized r^2	% drug release 60 min (Y_1)		Friability (Y_2)			
			r^2	SSE	r^2	SSE		
3	Training	0.4212	0.38	20.37	0.051	0.89		
	Testing	0.672	-0.02	37.93	0.681	.0063		
4*	Training	0.926	0.68	10.36	0.02	37.82		
	Testing	0.912	0.117	0.82	0.914	.0017		
5	Training	0.797	0.77	7.5	-0.07	39.66		
	Testing	0.332	0.089	0.84	0.37	0.0124		

*Node 4 is selected to generate the prediction profile as it has the overall highest r^2 value with minimum SSE

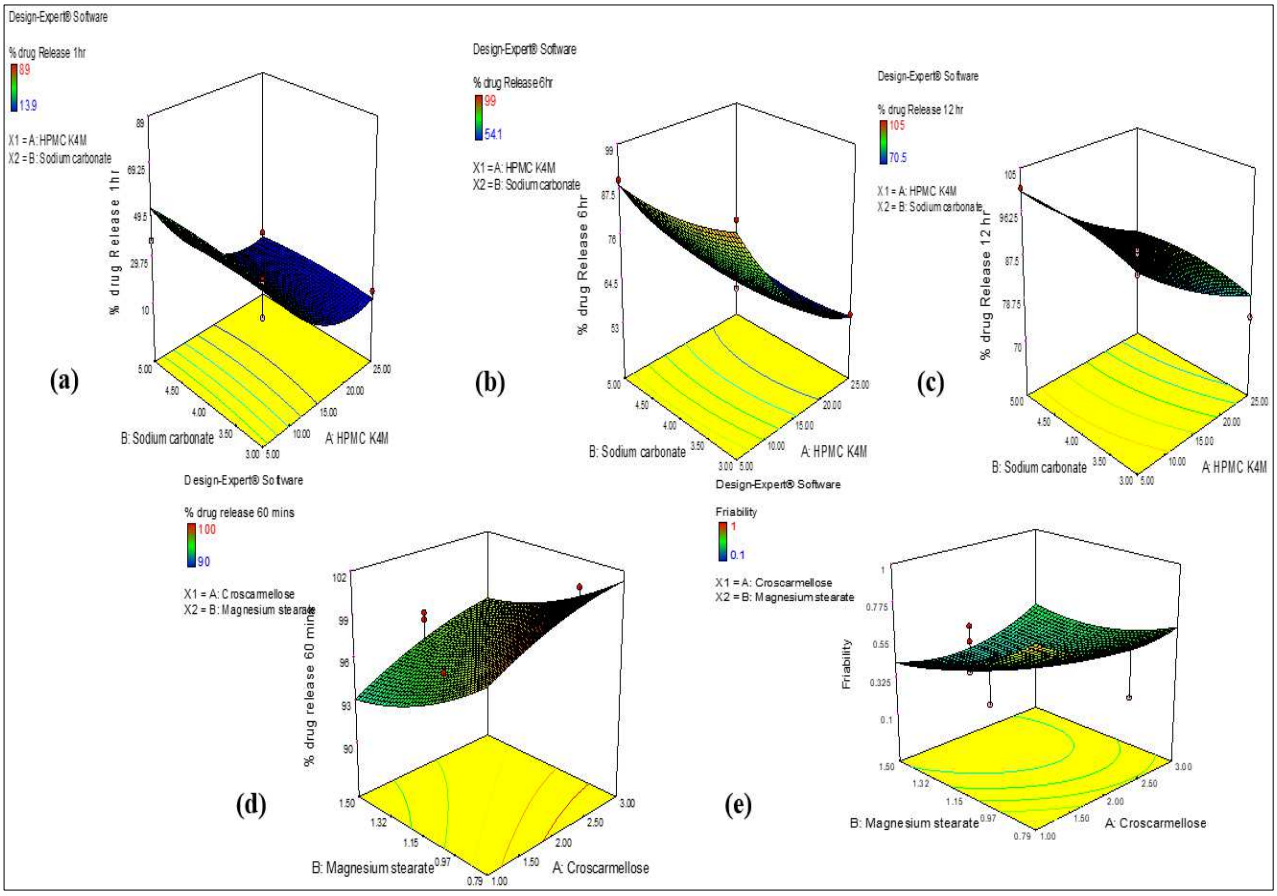

Fig. 6: Response surface plots (3D) originated from CCD presenting % drug release at 1h, 6h and12h (a,b,c) from ER formulations, % drug release at 1h and friability (d, e) from IR formulations

Table 7: Analysis of variance for the fitness of the central composite design matrix of both extended-release (CNZ) and immediate-release (DOM) formulations

Responses	Model	F-value	p-value	Model equations in terms of coded factors
		Extended-release (CNZ) formulations		
Y_1	Quadratic	7.81	0.0088	Y_1=18.51-18.65A+0.80B-0.75AB+13.72A^2-1.48 B^2
Y_2	Quadratic	107.94	0.0001	Y_2=64.00-17.06A+0.013B+1.25AB+6.65 A^2+2.34B^2
Y_3	Quadratic	29.87	.0001	Y_3=88.80-12.82A-2.35B-1.05AB-1.51A^2+1.62B^2
		Immediate-release (DOM) formulations		
Y_1	Quadratic	4.07	0.0472	Y_1=98.25+1.69A-4.26B+0.20AB-0.58A^2+1.65B^2
Y_2	Quadratic	0.62	0.6892	Y_2=0.48-0.054A-0.28B+0.1AB+0.11A^2+0.16 B^2

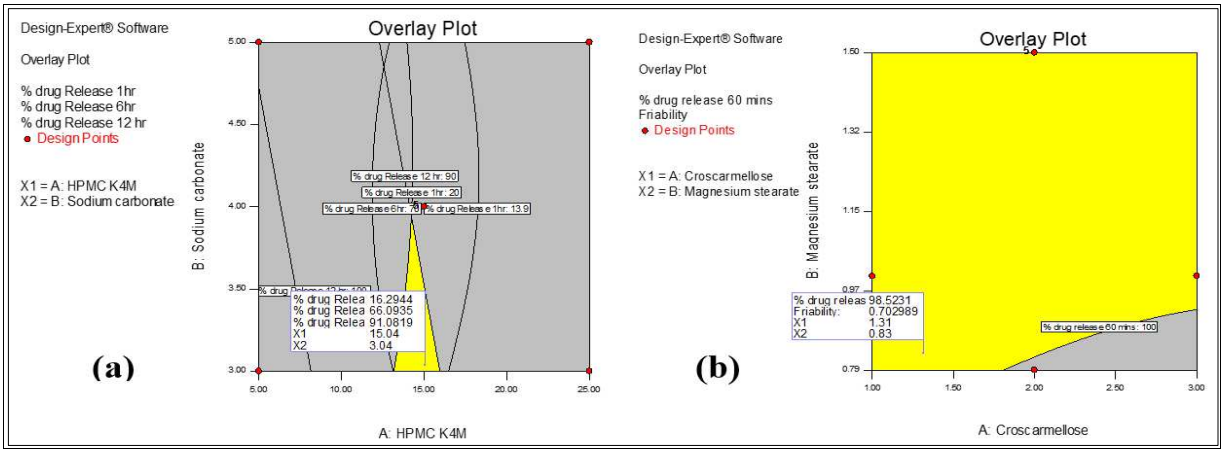

Fig. 7: Overlay plots obtained by graphical optimization exhibiting design space of (a) ER formulations (b) IR formulations

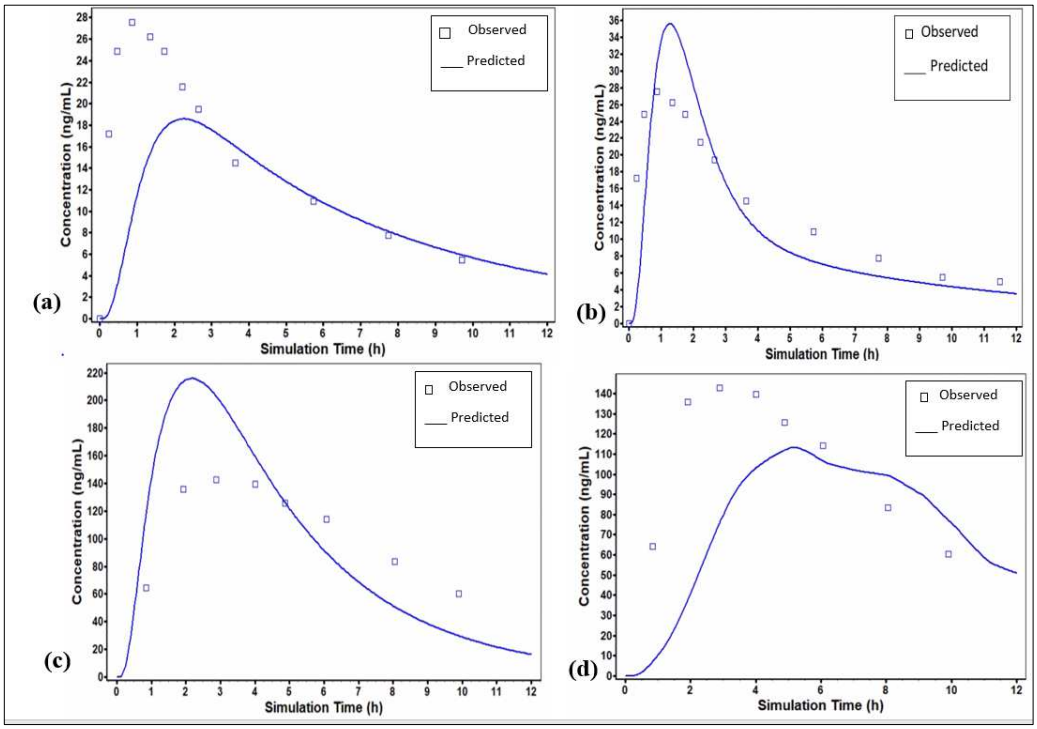

Fig. 8: Predicted and observed plasma concentration time curves: (a) Model building through extracted data from literature for domperidone (b) Model estimation for the optimized formulation, $F_{opt.\ CCD}$ (DOM) (c) Model building through extracted data from literature for cinnarizine (d) Model estimation for the optimized formulation, $F_{opt.\ CCD}$ (CNZ)

Table 8: ANOVA for the comparison of optimized and predicted formulations of both drugs originated from ANN and CCD

ER formulation[a]					
Source of variation	Sum of squares	Difference	Mean Square	F- value	p-value
Between groups	1.602	1	1.602	3.396	0.139
Within groups	1.887	4	0.472		
Total	3.488	5			
IR formulation[b]					
Between groups	1.530	1	1.530	1.839	0.247
Within groups	3.329	4	0.832		
Total	4.859	5			

[a]Group1: $F_{opt.\ CCD}$ (CNZ), Group 2: $F_{pred.\ ANN}$ (CNZ) [b]Group1: $F_{opt.\ CCD}$ (DOM), Group 2: $F_{pred.\ ANN}$ (DOM)

Table 9: Input parameters of both drugs for PBPK modeling

IR tablet (DOM)		
Parameters	Value	Source
Molecular weight (g/mol)	425.92	ADMET predictor®
Log P	3.96	ADMET predictor®
pKa	11.36, 8	ADMET predictor®
P_{eff} (cm/s×10^{-4})	1.55	ADMET predictor®
R_{bp} (Blood/plasma ratio)	0.8	ADMET predictor®
F_{up}(%)	3.92	ADMET predictor®
Precipitation time (s)	900	Gastroplus® standard
Diffusion coefficient (cm^2/sec×10^{-5})	0.64	ADMET predictor®
Drug particle density (g/ml)	1.2	ADMET predictor®
Physiology	Fasted (Human)	Experimental parameter
ASF (model)	Opt log D SA/V 6.1	Absorption scale factor
K_{12}(1/h)	1.52	PKPlus®
K_{21}(1/h)	0.25	PKPlus®
V_2(L/kg)	7.88	PKPlus®
ER tablet (CNZ)		
Molecular weight (g/mol)	368.514 g/mol	ADMET predictor®
Log P	5.6	((Kesharwani and Ibrahim, 2023)
pKa	1.95, 7.47	((Kesharwani and Ibrahim, 2023)
P_{eff} (cm/s×10^{-5})	1.63	(Kesharwani and Ibrahim, 2023)
R_{bp} (Blood/plasma ratio)	1	(Berlin *et al*., 2014)
F_{up}(%)	0.165	ADMET Predictor®
Precipitation time (s)	900	Gastroplus™ Standard
Diffusion coefficient (cm^2/sec×10^{-5})	0.62	ADMET predictor®
Drug particle density (g/ml)	1.2	ADMET predictor®
Physiology	Fasted (Human)	Experimental parameter
ASF (model)	Opt log D SA/V 6.1	Absorption scale factor
Cl (L/h)	5.02	PKPlus®
V_c(L/kg)	3.99	PKPlus®

The physiological and physicochemical parameters were computed using the ADMET® predictor embedded in the software and were also retrieved from the literature. The plasma concentration-time profiles extracted from previous studies were included in the PK Plus® module of Gastroplus®. This module evaluated the input data using one, two, and three-compartment models (Wang *et al*., 2023).

Model evaluation and simulation

The developed model was evaluated by calculating fold error (FE) for C_{max}, T_{max}, $AUC_{0\text{-}inf,}$ and $AUC_{0\text{-}t}$. The *in-vitro* dissolution profiles of both drugs were entered, and a single simulation was performed. Relative bioavailability was also calculated for both drugs.

RESULTS

Pre-compression and post-compression studies

The findings of micrometrics studies complied with the USP specifications mentioned in General Chapter <1174> Powder Flow (USP-NF, 2022) and compiled in table 3, while the results of post-compression quality control evaluation were given in table 4, representing FD1-FD13 (IR formulations), F1-F13 (ER formulations), and B1 (bilayer formulation). The FTIR spectra of individual drugs

(Fig. 1a and 1c) along with the blended polymer (HPMC K4M) and superdisintegrant (croscarmellose) are displayed in fig. 1(b) and (d). The cumulative % drug release time profile curves of domperidone and cinnarizine are presented in fig. 2(a) and (b), respectively. The chromatograms of standard domperidone and cinnarizine, along with their optimized bilayer tablets, are also illustrated in fig. 2(c) and (d), respectively. The mechanism of drug release kinetics of the ER and IR formulations, after applying different kinetic models and f_2 values, is presented in table 5.

ANN-based modeling

The MLP neural network built with input variables (HPMC K4M and sodium carbonate) and dissolution time points as output responses with one hidden layer containing 3, 4 and 5 activation nodes in the case of ER formulations, is illustrated in fig. 3. Similarly, the MLP neural network also designed for the IR formulations with croscarmellose and magnesium stearate as input variables, is also displayed in fig. 3. The performance indices of training and testing of data in terms of r^2 and SSE values for both drugs are compiled in table 6.

Optimization based on the prediction profiler originated from the ANN

The generated prediction profiles in figs. 4(a) and (c) indicate the predicted values of the independent variables against the targeted responses, which are found to be close to the values as obtained by CCD-based numerical optimization (Fig. 5). Along with prediction profilers, contour profilers for both drugs were also computed and presented in figs. 4(b) and (d).

CCD-based modeling

The experimental data from the CCD-generated trial formulations (F1-F13) and (FD1-FD13) were used with the numerical optimization technique of central composite design to predict the values of the input variables, which are presented in the ramp plots (Fig. 5) showing desirability that almost meets the target goals. The CCD-generated optimized formulations, as shown in the ramp plots for cinnarizine and domperidone, are denoted $F_{opt.\ CCD}$ (CNZ) and $F_{opt.\ CCD}$ (DOM), respectively, which were subsequently selected for the development of the bilayer tablet. The polynomial equations, along with selected models, are presented in table 7. The effects of input variables on the output responses are also given by constructing 3D response surface plots in fig. 6. The overlay plots from the graphical optimization are shown in fig. 7, which illustrate the yellow area as the design space.

ANOVA-based comparison between CCD and ANN-assisted formulations

In recent work, the model efficiency of both techniques (CCD and ANN) was assessed using an ANOVA-based comparison. The one-way analysis of variance indicated no significant differences between the optimized formulations assisted by CCD and the predicted formulations originated by ANN in terms of critical output responses. The p-values for ER and IR tablets were 0.139 and 0.247, respectively, as shown in table 8.

In-silico PBPK study

The input parameters retrieved from the literature and predicted by the ADMET® are presented in table 9. The pharmacokinetic parameters determined by the PKPlus® module from the available reported studies, including C_{max}, T_{max}, $AUC_{0\text{-}inf}$, and $AUC_{0\text{-}t}$, along with fold errors, are listed in table 10. The model also selected a two-compartment model for domperidone, while a one-compartment model for cinnarizine. Fig. 8 depicts the visual resemblance between the predicted and the experimental (observed) profiles.

DISCUSSION

This study aimed to identify the critical input variables by simultaneously applying a ML-based ANN model and a conventional RSM-based CCD model to each formulation (i.e., IR and ER), followed by the development of a bilayer tablet using the resultant optimized compositions. The FTIR study indicated compatibility of cinnarizine with the polymer and of domperidone with the superdisintegrant, as reported by other studies (Oransa *et al*., 2022; Lee *et al*., 2014). All trial batches and the optimized formulations were subjected to physicochemical evaluation in accordance with USP and in-house quality control testing. The average weight variation results of all the IR and ER tablets (Table 4) complied with the pharmacopoeial limits, i.e., ±7.5% with 200mg as the target weight. Similarly, the average weight variation of all the bilayer tablets (Table 4) was within USP limits, i.e., ±5%, while targeting an average weight of 400mg. The hardness of all the ER tablets of cinnarizine and IR tablets of domperidone were in the range of 5.5±0 to 6.8±0.1kg/cm^2 and 3.1±0.1 to 4.6±0.2 kg/cm^2, respectively. The hardness of the compressed bilayer tablets ranged from 7.7±0.12 to 8.6±0.2 kg/cm^2. The friability of all IR, ER, and bilayer tablets was recorded as less than 1%, thereby complying with the specifications (USP-NF, 2022). The in-vitro dissolution data for the trial batches were assessed for release kinetics using both model-dependent and model-independent approaches. The r^2 values were in a range between 0.01-0.85 (zero-order), 0.48-0.99 (first-order), 0.6-0.98 (Higuchi), 0.87-0.99 (Korsmeyer-Peppas), and 0.76-0.98 (Hixson-Crowell). Compared with other models, the Korsmeyer-Peppas model provided the best fit. The release exponent, "n", of formulations coded F4, F10, and F11 was found to be less than 0.45, indicating Fickian diffusion.

Table 10: Pharmacokinetic (Pk) parameters obtained from the observed and predicted plasma concentration profile following oral administration of domperidone and cinnarizine

Pk parameters domperidone	Oral tablet (20mg DOM)			Fopt. CCD (15mg DOM)	
	Observed	Predicted	FE*	Predicted	FE*
C_{max} (ng/ml)	27.5	35.59	1.29	24.10	1.14
T_{max} (h)	0.89	1.28	1.43	1.28	0.67
$AUC_{0\text{-}inf}$ (ng-h/ml)	231.5	164.42	0.71	115.98	1.99
$AUC_{0\text{-}t}$ (ng-h/ml)	144.5	131.07	0.90	88.4	1.63
Pk parameters cinnarizine	Oral tablet (75mg CNZ)			Fopt. CCD (75 mg CNZ)	
	Observed	Predicted	FE*	Predicted	FE*
C_{max} (ng/ml)	142.6	215.8	1.51	110.69	1.28
T_{max} (h)	2.88	2.16	0.75	5.08	0.56
$AUC_{0\text{-}inf}$ (ng-h/ml)	1361	1200	0.88	1336	1.01
$AUC_{0\text{-}t}$ (ng-h/ml)	1014	1144	1.12	905.35	1.12

*Fold Error (FE) = Predicted/Observed (Li *et al*., 2024)

Incontrast, formulations coded as F1, F2, F3, F5, F6, F7, F8, F9, F12 and F13 exhibited higher "n" values. These findings are consistent with previous studies by Kriangkrai et al. and Nagarwal et al., which suggest non-Fickian diffusion from a matrix tablet containing HPMC as the release-controlling polymer (Kriangkrai *et al*., 2024; Nagarwal *et al*., 2024). All the trial formulations of IR tablets were best fit to first-order kinetics (0.9122-0.9889), whereas weak correlation coefficients were observed for the Hixson-Crowell model (0.50-0.857). Similar results were reported in a study in which domperidone followed first-order kinetics when formulated as an immediate-release layer of a bilayer tablet, suggesting that dissolution of the drug was the predominant mechanism, rather than diffusion, swelling, erosion, or relaxation due to matrix formation of the polymer (Prajapati *et al*., 2024). The drug content was found to be within 85% to 115% as per specification (BP, 2022).

To leverage the artificial intelligence in this study, JMP® Pro is used to build an artificial neural network. The input layer of this network receives the initial data for two independent variables —HPMC (K4M) and sodium carbonate —and passes it to the hidden layer, which lies between the input and output layers. The hidden layer transforms the data before processing towards the output layer which represents the outcomes, namely % drug release at 1h, 6h and 12h after processing the data through ANN as demonstrated in fig. 3. The same neural network was constructed in the case of IR formulations (Fig. 3). The optimal performance was achieved with 4 neurons in the hidden layer activated by TanH function using a 0.1 learning rate and the square penalty method in the current study. In one of the studies conducted by El-Metwally, the best ANN architecture was built using a 0.1-squared learning method, with three layers and a holdback ratio of 0.3333, which divided the data into 10 training runs, thereby reducing prediction errors and enabling the calculation of neural weights. The remaining 5 validation runs serve to halt the training process. The study revealed that the model was trained until r2 reached 0.9933, a value associated with the model's generalizability (El-Metwally *et al*., 2023). In another study, Sheth and Acharya also employed an artificial neural network to optimize the drug-release profile of quetiapine fumarate MR tablets. During the training process, the excipient weights were optimized to achieve the target drug release using MATLAB® software (Sheth and Acharya, 2024).

The literature indicates that the built-in prediction profiler function in JMP® Pro can examine the influence of variation in independent factors on dependent factors, thereby identifying the optimal combination of input variables that maximizes desirability (Puri *et al*., 2022). Similarly, after model training and testing, the built-in model profiler is used in this study to select nodes and predict optimal levels of input variables. In the case of the ER formulation (Table 6), nodes 3 and 4 both show good overall generalized coefficients of correlation, but node 3 is found to be inconsistent as it fails to predict Y_3 response with a nearly zero r^2 value and is also accompanied by a high value of SSE, therefore not suitable to generate a complete profile. Moreover, the negative r^2 for the Y_1 response at node 5 demonstrates its insufficiency to predict the key response, while the r^2 values for all three responses (Y1, Y2, and Y_3) are high and very close to each other (0.83-0.86), indicating consistency at node 4. Similarly, in the case of the IR formulation, node 3 shows a low generalized correlation coefficient in both the testing (r^2=0.4212) and training (r^2=0.672) datasets, indicating underfitting, while node 4 is superior, with r^2=0.926 (training) and r^2=0.912 (testing). Moreover, the subsequent node 5 shows good training (r^2=0.797), but fails to demonstrate good generalization capability in the testing phase (r^2=0.332). Therefore, further training was halted, and a prediction profile was generated at node 4 (Fig. 4). The SSE values at node 4 are not the lowest for each parameter, but the overall coefficient of correlation was found to be highest in both the testing and training phases.

The desirability value achieved through numerical optimization using CCD is the ideal value as shown in the ramp plot fig. 5 (a) and (b); however, the desirability values, i.e., 0.889 (Fig. 4a) and 0.716 (Fig. 4c), acquired through prediction profiler using ANN-MLP, are also close to the desired value. In one of the studies conducted by Kumar *et al*. obtained a desirability of 0.809 after generating a prediction profile, indicating an optimal level of independent variables including HPMC 15cps (40%), PEG 400 (10%) and teen 80 (1%) predicting % drug release in 15 minutes (96.22 %), % drug content (95.96%), disintegration time (26.5sec.) and folding endurance (278.25) for the development of fast dissolving buccal film of ivabradine (Kumar *et al*., 2024). The 3D surface plots in fig. 6 (a-e) show pronounced curvatures that explicitly link with the non-linear relationship between the independent and all the dependent factors of both ER and IR formulations. Another study also indicated a curve response in 3D plots between the factors, illustrating a non-linear effect (Bangera *et al*., 2025).

A CCD-assisted multi-criteria decision strategy of numerical optimization targeting the desirability approach close to 1, also employed to achieve the desired quality attributes by optimizing the input variables of both ER and IR tablets. The quadratic model was found to be the best fit as per the ANOVA fit summary (Table 7). To assess the adequacy and efficiency of both predictive models, i.e., CCD and ANN, a one-way ANOVA was performed. The statistical insignificance ($p>0.05$) indicated similarities in the output responses (% drug release at 1h, 6h, and 12h for the ER layer, and % drug release at 1h and % friability for the IR layer). The results support the introduction of machine learning programs as an optimization technique, which are consistent with those reported by Khan et al. and Saleem et al. for the QbD-based formulation of moxifloxacin orodispersible and rivaroxaban push-pull osmotic tablets, respectively (Khan *et al*., 2023; Saleem *et al*., 2025).

The ACAT® model was initially developed by comparing the predicted plasma concentration-time profile with the experimental values following oral administration of 20 mg domperidone in healthy male volunteers (Helmy and El Bedaiwy, 2014), as the intravenous plasma concentration-time profile is not readily accessible. The same procedure was followed for the extended-release cinnarizine formulation, using data from the literature (Morrison *et al*., 1979). In fig. 8, the plasma concentration-time plot of predicted and experimental values overlaps for domperidone, whereas the predicted curve for the optimized formulation of cinnarizine resembles the reported study (Kesharwani and Ibrahim, 2023). However, the predicted parameters, including C_{max} (ng/ml), T_{max} (h), $AUC_{0\text{-}inf}$ (ng-h/ml), and $AUC_{0\text{-}t}$ (ng-h/ml), were within the 2-fold error range, as per specifications, which assures good predictive performance (Cho *et al*., 2022). The relative bioavailability of the CCD-generated formulations of cinnarizine (89%) and domperidone (81%) was within the acceptable range, i.e., 80-125% (Amini *et al*., 2020).

CONCLUSION

In this study, a neural network-based ANN model was successfully built, trained, and implemented to achieve the desired quality attributes of the bilayer tablet formulation with cinnarizine and domperidone as model drugs. The predicted formulation obtained by the trained ANN architecture was successfully cross-validated by the multivariate CCD approach. Based on *in-silico* PBPK studies, the oral bioavailability of the two drugs can be readily understood along with the specific inter-personal pharmacokinetic diversity without conducting *in-vivo* studies.

Acknowledgment
The authors would like to thank Simulation Plus and SAS Institute for granting an academic research license to use GastroPlus® and JMP® Pro 18 for non-commercial academic research. The authors are also very grateful to the Department of Pharmaceutics, Faculty of Pharmacy and Pharmaceutical Sciences, University of Karachi, for providing laboratory facilities.

Authors' contributions
Aatka Ali: Original draft preparation, experimentation, investigation, and software.
Iyad Naeem Muhammad: Conceptualization, supervision, writing, reviewing, and editing
Wajiha Iffat: Supervision, methodology writing- reviewing
Shumaila Tasneem: Investigation and resources.
Syed Ahsan Ali: Investigation and resources.
Sarah Jameel Khan: Investigation and resources.
Sidra Siddique: Investigation, resources.

Funding
There was no funding.

Data availability statement
The data of this study are available from the corresponding author upon reasonable request.

Ethical approval
Not applicable

Conflict of interest
There is no conflict of interest.

REFERENCES

Afzal M, Muddassir M, Alarifi A and Ansari MTJS (2021). Box-Behnken assisted validation and optimization of an RP-HPLC method for simultaneous determination of domperidone and lansoprazole. *Separations,* **8**(1): 5.

Akhtar M, Zaman M, Siddiqi AZ, Ali H, Khan R, Alvi MN, Butt MH, El-Demerdash FM, Binjawhar DN and Sayed AA (2024). Response surface methodology (RSM)

approach to formulate and optimize the bilayer combination tablet of tamsulosin and finasteride. *Saudi Pharm. J.,* **32**(3): 101957.

Alam P and Shakeel F (2024). Simultaneous determination of cinnarizine and domperidone in marketed tablets using a green HPTLC method. *Acta Chromatogr.,* **37**(3): 307-317.

Altoum GH, Al-Enazi FK, Abudahash MM, Al-Fadhli RA and Alenzi N (2024). A comparative study on vildagliptin brand and its generic equivalents using dissolution test as quality control measure tool. *Sci. Rep.,* **14**(1): 2636.

Amini M, Reis M and Wide-Swensson D (2020). A relative bioavailability study of two misoprostol formulations following a single oral or sublingual administration. *Front. Pharmacol.,* **11**: 50.

Ardalkar S, Mathure D, Pawar A & Awasthi R (2024). Formulation and optimization of electrospun nanofiber films for ultrafast delivery of domperidone: *In vitro* and in-vivo characterization. *J. Drug Deliv. Sci. Technol.,* **95**: 105645.

Asrade B, Tessema E and Tarekegn A (2023). *In-vitro* comparative quality evaluation of different brands of carbamazepine tablets commercially available in Dessie town, Northeast Ethiopia. *BMC Pharmacol. Toxicol.,* **24**(1): 35.

Bangera PD, Lobo KN, Keerikkadu M, Kara DD, Tippavajhala VK and Rathnanand M (2025). Development, optimization and characterization of ibrutinib-loaded chitosomes using box-behnken design: *In-vitro* evaluation and in vivo pharmacokinetic studies. *BioNanoScience,* **15**(3): 384.

Berlin M, Przyklenk KH, Richtberg A, Baumann W and Dressman JB (2014). Prediction of oral absorption of cinnarizine–a highly supersaturating poorly soluble weak base with borderline permeability. *Eur. J. Pharm. Biopharm.,* **88**(3): 795-806.

British Pharmacopoeia 2022*,* London, Stationery Office.

Cho CK, Kang P, Park HJ, Ko E, Mu CY, Lee YJ, Choi CI, Kim HS, Jang CG and Bae JW (2022). Physiologically based pharmacokinetic (PBPK) modeling of piroxicam with regard to CYP2C9 genetic polymorphism. *Arch. Pharm. Res.,* **45**(5): 352-366.

Conemans, J. M. H. 2011. Systems for drug analysis. *In:* Moffat, A. C., Osselton, M. D., Widdop, B. & Watts, J. (editors). Clarke's analysis of drugs and poisons. 3rd ed., London: Pharmaceutical Press, p.517.

Demeester C, Robins D, Edwina AE, Tournoy J, Augustijns P, Ince I, Lehmann A, Vertzoni M and Schlender JF (2023). Physiologically based pharmacokinetic (PBPK) modelling of oral drug absorption in older adults–an AGePOP review. *Eur. J. Pharm. Sci.,* **188**: 106496.

Diaz DA, Colgan ST, Langer CS, Bandi NT, Likar MD and Van Alstine L (2016). Dissolution similarity requirements: how similar or dissimilar are the global regulatory expectations? *AAPS J.,* **18**: 15-22.

El-Metwally MM, Abdel-Fattah GM, Al-Otibi FO, Khatieb DKE, Helmy YA, Mohammed YM and Saber WI (2023). Application of artificial neural networks for enhancing *Aspergillus flavipes* lipase synthesis for green biodiesel production. *Heliyon,* **9**(9): e20063.

Elsayed MS, Eldadamony NM, Alrdahe SS and Saber WI (2021). Definitive screening design and artificial neural network for modeling a rapid biodegradation of date palm fronds by a new Trichoderma sp. PWN6 into citric acid. *Molecules,* **26**(16): 5048.

Freriksen JJ, Van Der Heijden JE, De Hoop-Sommen MA, Greupink R and De Wildt SN (2023). Physiologically based pharmacokinetic (PBPK) model-informed dosing guidelines for pediatric clinical care: A pragmatic approach for a special population. *Paediatr. Drugs,* **25**(1): 5-11.

Harkat-Madouri L, Touati H, Boulekbache-Makhlouf L, Madani K and Haddadi-Guemghar H (2025). Optimization of the microwave-assisted extraction of total phenolic compounds (TPCs) from almond skins through artificial neural networks (ANNs) and assessment of the antioxidant and antihyperglycemic activity of the extracts. *J. Food Process. Preserv.,* **2025**(1): 3294168.

Helmy SA and El Bedaiwy HM (2014). Pharmacokinetics and comparative bioavailability of domperidone suspension and tablet formulations in healthy adult subjects. *Clin. Pharmacol. Drug Dev.,* **3**(2): 126-131.

Huang H, Zhao W, Qin N and Duan X (2024). Recent progress on physiologically based pharmacokinetic (PBPK) model: A review based on bibliometrics. *Toxics,* **12**(6): 433.

Ismail MA, Mohd Azam NN, Mohamad MS, Ibrahim AO and Jeba S (2023). Classification of COVID-19 symptoms using multilayer perceptron. *Iraqi J. Comput. Sci.,* **4**(4): 99-110.

Kesharwani SS and Ibrahim F (2023). A combined in-vitro and GastroPlus® modeling to study the effect of intestinal precipitation on cinnarizine plasma profile in a fasted state. *AAPS PharmSciTech.,* **24**(5): 121.

Khan MZ, Yousuf RI, Shoaib MH, Ahmed FR, Saleem MT, Siddiqui F and Rizvi SA (2023). A hybrid framework of artificial intelligence-based neural network model (ANN) and central composite design (CCD) in quality by design formulation development of orodispersible moxifloxacin tablets: Physicochemical evaluation, compaction analysis and its in-silico PBPK modeling. *J. Drug Deliv. Sci. Technol.,* **82**: 104323.

Kriangkrai W, Puttipipatkhachorn S, Sriamornsak P & Sungthongjeen S (2024). Design and evaluation of new gel-based floating matrix tablets utilizing the sublimation technique for gastroretentive drug delivery. *Gels,* **10**(9): 581.

Kumar AS, Reddy KAN, Reddy RN, Reddy KS and Dang R (2024). Quality by design assisted development of fast dissolving buccal film of ivabradine. *Iraqi J. Comput. Sci.,* **58**(2s): s484-s501.

Lee JH, Kim MJ, Yang J, Kim KH, Kim HM, Lee SJ, Lee D and Khang G (2014). Enhancing dissolution of domperidone by spray-drying: Effect of different storage conditions on stability. *Ther. Deliv.,* **5**(3): 265-275.

Li Y, Wang Z, Li Y, Du J, Gao X, Li Y and Lai L (2024). A combination of machine learning and PBPK modeling approach for pharmacokinetics prediction of small molecules in humans. *Pharm. Res.,* **41**(7): 1369-1379.

Lin W, Chen Y, Unadkat JD, Zhang X, Wu D and Heimbach T (2022). Applications, challenges and outlook for PBPK modeling and simulation: A regulatory, industrial and academic perspective. *Pharm. Res.,* **39**(8): 1701-1731.

Makomere R, Rutto H and Koech L (2023). The assessment of response surface methodology (RSM) and artificial neural network (ANN) modeling in dry flue gas desulfurization at low temperatures. *J. Environ. Sci. Health A.,* **58**(3): 191-203.

Malenga EN, Mulaba-Bafubiandi A and Nheta W 2022. Application of the response surface method (RSM) based on central composite design (CCD) and design space (DS) to optimize the flotation and the desliming conditions in the recovery of PGMs from mine sludge. *Sep. Sci. Technol.,* **57**(18): 2960-2983.

Maqbool T, Yousuf RI, Ahmed FR, Shoaib MH, Irshad A, Saleem MT, Qazi F, Sarfaraz S, Rizvi SA and Mahmood ZA (2024). Cellulose ether and carbopol 971 based gastroretentive controlled release formulation design, optimization and physiologically based pharmacokinetic modeling of ondansetron hydrochloride minitablets. *Int. J. Biol. Macromol.,* **276**: 133841.

Mazumdar D, Saha SP and Ghosh S (2021). RSM based optimization of plant growth promoting rhizobacteria and nitrogen dosage for enhanced growth and yield of mustard (*Brassica campestris* L.). *J. Plant Nutr.,* **44**(15): 2228-2244.

Morrison P, Bradbrook I and Rogers H (1979). Plasma cinnarizine levels resulting from oral administration as capsule or tablet formulation investigated by gasliquid chromatography. *Br. J. Clin. Pharmacol.,* **7**(4): 349-352.

Nagarwal, R. C., Ridhurkar, D. N. & Pandit, J. 2010. In vitro release kinetics and bioavailability of gastroretentive cinnarizine hydrochloride tablet. *AAPS PharmSciTech,* **11**(1): 294-303.

Navabhatra A, Brantner A and Yingngam B (2021). Artificial neural network modeling of nanostructured lipid carriers containing 5-O-caffeoylquinic acid-rich Cratoxylum formosum leaf extract for skin application. *Adv. Pharm. Bull.,* **12**(4): 801.

Nguyen NNT, Pham DT, Nguyen DT and Trinh TTL (2021). Bilayer tablets with sustained-release metformin and immediate-release sitagliptin: Preparation and *in-vitro*/ *in-vivo* evaluation. *J. Pharm. Investig.,* **51**(5): 579-586.

Oransa HA, Boughdady MF and El-Sabbagh HM (2022). Novel mucoadhesive chitosomes as a platform for enhanced oral bioavailability of cinnarizine. *Int. J. Nanomed.,* **17**: 5641.

Paneiro G and Rafael M (2021). Artificial neural network with a cross-validation approach to blast-induced ground vibration propagation modeling. *Undergr. Space,* **6**(3): 281-289.

Pham BT, Nguyen MD, Bui KTT, Prakash I, Chapi K and Bui DT (2019). A novel artificial intelligence approach based on multilayer perceptron neural network and biogeography-based optimization for predicting coefficient of consolidation of soil. *Catena,* **173**: 302-311.

Prajapati R, Kumar B, Sahoo J, Shakya S and Lal DK (2024). Quality by design approach for the formulation of bilayer tablets of domperidone and itopride in gastro-esophageal reflux disease. *J. Appl. Pharm. Sci.,* **14**(8): 169-181.

Prajapati S, Patel L and Patel D (2009). Studies on formulation and *in-vitro* evaluation of floating matrix tablets of domperidone. *Indian J. Pharm. Sci.,* **71**(1): 19.

Puri V, Froelich A, Shah P, Pringle S, Chen K and Michniak-Kohn B (2022). Quality by design guided development of polymeric nanospheres of terbinafine hydrochloride for topical treatment of onychomycosis using a nano-gel formulation. *Pharmaceutics,* **14**(10): 2170.

Rojek B, Gazda M and Plenis A (2023). FTIR, Raman spectroscopy and HT-XRD in compatibility study between naproxen and excipients. *Spectrochim. Acta A Mol. Biomol. Spectrosc.,* **302**: 123048.

Saleem MT, Shoaib MH, Yousuf RI and Siddiqui F (2025). RSM and AI based machine learning for quality by design development of rivaroxaban push-pull osmotic tablets and its PBPK modeling. *Sci. Rep.,* **15**(1): 7922.

Sheth TS and Acharya F (2024). Optimization and evaluation of modified release solid dosage forms using artificial neural network. *Sci. Rep.,* **14**(1): 16358.

Simoes MF, Silva G, Pinto AC, Fonseca M, Silva NE, Pinto RM and Simoes S (2020). Artificial neural networks applied to quality-by-design: From formulation development to clinical outcome. *Eur. J. Pharm. Biopharm.,* **152**: 282-295.

United States Pharmacopeia and National Formulary (USP–NF) 2022. Rockville, MD, United States Pharmacopeial Convention.

Vyas K and Taft DR (2025). PBPK modeling for enhanced drug therapy in the elderly population and the impact of organ impairment on systemic exposure. *Curr. Pharmacol. Rep.,* **11**(1): 10.

Wang L, Hu Q, Wang L, Shi H, Lai C and Zhang S (2022a). Predicting the growth performance of growing-finishing pigs based on net energy and digestible lysine intake using multiple regression and artificial neural networks models. *J. anim. sci. biotechnol.,* **13**(1): 57.

Wang L, Zhao P, Luo T, Yang D, Jiang Q, Chen J, Lou H, Ruan Z and Jiang B (2023). Physiologically based absorption modeling to predict the bioequivalence of two cilostazol formulations. *Clin. Transl. Sci.,* **16**(11): 2323-2330.

Wang S, Di J, Wang D, Dai X, Hua Y, Gao X, Zheng A and Gao J (2022b). State-of-the-art review of artificial neural networks to predict, characterize and optimize pharmaceutical formulation. *Pharmaceutics,* **14**(1): 183.

Yu LX and Amidon GL (1999). A compartmental absorption and transit model for estimating oral drug absorption. *Int. J. Pharm.,* **186**(2): 119-125.

Zhang Y, Li Q, Wang C, Zhu L, Wang F, Jiao W, Zhuang X, Xie F, Du L and Jin Y (2022). Cinnarizine dissolving microneedles against microwave-induced brain injury. *Biomed. Pharmacother.,* **155**: 113779.